

MisMatch: Learning to Change Predictive Confidences with Attention for Consistency-Based, Semi-Supervised Medical Image Segmentation

Mou-Cheng Xu, Yu-Kun Zhou, Chen Jin, Stefano B. Blumberg, Frederick J. Wilson, Marius De Groot, Neil P. Oxtoby, Daniel C. Alexander and Joseph Jacob

Abstract—The lack of labels is one of the fundamental constraints in deep learning based methods for image classification and segmentation, especially in applications such as medical imaging. Semi-supervised learning (SSL) is a promising method to address the challenge of label scarcity. The state-of-the-art SSL methods utilise consistency regularisation to learn unlabelled predictions which are invariant to perturbations on the prediction confidence. However, such SSL approaches rely on hand-crafted augmentation techniques which could be sub-optimal. In this paper, we propose MisMatch, a novel consistency based semi-supervised segmentation method. MisMatch automatically learns to produce paired predictions with increased and decreased confidences. MisMatch consists of an encoder and two decoders. One decoder learns positive attention for regions of interest (RoI) on unlabelled data thereby generating higher confidence predictions of RoI. The other decoder learns negative attention for RoI on the same unlabelled data thereby generating lower confidence predictions. We then apply a consistency regularisation between the paired predictions of the decoders. For evaluation, we first perform extensive cross-validation on a CT-based pulmonary vessel segmentation task and show that MisMatch statistically outperforms state-of-the-art semi-supervised methods when only 6.25% of the total labels are used. Furthermore MisMatch performance using 6.25% of the total labels is comparable to state-of-the-art methods that utilise all available labels. In a second experiment, MisMatch outperforms state-of-the-art methods on an MRI-based brain tumour segmentation task.

Index Terms—Visual Attention, Confidence Calibration, Semi-Supervised Learning, Segmentation

MCX is supported by GlaxoSmithKline (BIDS3000034123) via UK EPSRC CDT in i4Health and UCL Engineering Dean's Prize. NPO is supported by a UKRI Future Leaders Fellowship (MR/S03546X/1). DCA is supported by UK EPSRC grants M020533, R006032, R014019, V034537, Wellcome Trust UNS113739. JJ is supported by Wellcome Trust Clinical Research Career Development Fellowship 209,553/Z/17/Z. NPO, DCA, and JJ are supported by the NIHR UCLH Biomedical Research Centre, UK.

MCX, YKZ, CJ, SBB, NPO, DCA, JJ are with Centre for Medical Image Computing, UCL, UK. MXC, YKZ are with Department of Medical Physics and Biomedical Engineering, UCL, UK. CJ, SBB, NPO, DCA are with Department of Computer Science, UCL, UK. FJW and MDG are with GlaxoSmithKline Research & Development, Stevenage, UK. JJ is with University College London Hospital, UK.

Author contact: <https://moucheng2017.github.io/>

I. INTRODUCTION

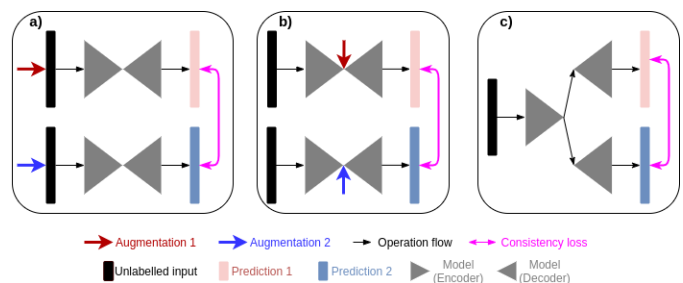


Fig. 1. Different strategies for consistency regularisation. (a) Previous methods [32, 31, 11] use hand-crafted augmentation at input level to create predictions with different confidences. (b) Previous method [28] uses hand-crafted augmentation at feature level to create predictions with different confidences. (c) Our method end-to-end learns to create predictions with different confidences.

Training of deep learning models requires a large amount of labelled data. However, in applications such as in medical image analysis, anatomic/pathologic labels are prohibitively expensive and time-consuming to obtain, with the result that label scarcity is almost inevitable. Advances in the medical image analysis field requires the development of label efficient deep learning methods and accordingly, semi-supervised learning (SSL) has become a major research interest within the community. Among the myriad SSL methods used, consistency regularisation based methods have achieved the state-of-the-art in classification [32, 31, 2, 1], thus we focus on this genre in this paper.

Existing consistency regularisation methods [32, 31, 2, 1, 28, 16, 11, 22] can be considered as two-stages pipelines. In the first stage they apply different augmentation techniques at the input level (Fig1(a)) or the feature level (Fig1(b)) to change the prediction confidences. For example, if we apply weak augmentation such as flipping on an input image, the model will assign a high probability of this image belonging to its correct label, hence, the prediction of the weakly augmented image is with high confidence; if we apply strong augmentation such as rotation on an input image, then the testing is much more difficult and the model might assign a low probability of this image to its correct label, therefore,

such a prediction of a strongly augmented image is with low confidence. In the second stage of the pipeline, a consistency regularisation is enforced to align the paired predictions. However, such data augmentation techniques are typically hand-crafted which might be sub-optimal. More importantly, such augmentation techniques are not adaptive across pixels which may be problematic as spatial correlations amongst pixels are crucial for segmentation, e.g. neighbouring pixels might belong to the same category.

In this paper, we reframe SSL with consistency regularisation as a single-stage learning problem and we propose an end-to-end learning framework to generate predictions with different confidences (Fig 1 (c)). In order to change prediction confidences at a pixel-wise level in a realistic way, we use two different attention mechanisms to respectively increase and decrease prediction confidences of the entire foreground regions of interest (RoIs) which represent areas of “ground truth”. We intensively evaluate MisMatch on two medical applications: first a CT-based lung vessel segmentation task where MisMatch outperforms several benchmarks; second, we confirm the effectiveness of MisMatch on a MRI-based brain tumour segmentation task. **The code will be released after reviewing.**

II. RELATED WORK

SSL in classification A recent review [27] summarised different common SSL [15] [26] [32] methods including entropy minimisation, label propagation methods, generative methods and consistency based methods. Entropy minimisation encourages models to produce less confident predictions on unlabelled data [12] [20]. However, entropy minimisation might overfit to the clusters of classes and fail to detect the decision boundaries of low-density regions (see Appendix E in [27]). Label propagation methods [15] [20] aim to build a similarity graph between labelled data points and unlabelled data points in order to propagate labels through dense unlabelled data regions. Nevertheless, label propagation methods need to build and analyse their Laplacian matrices which will limit their scalability. Generative models have also been used to generate more data points in a joint optimisation of both classification of labelled data points and generative modelling [19]. However, the training of such a joint model can be complicated and unstable. On the other hand, consistency regularisation methods have achieved state-of-the-art performances across different benchmarks, additionally, consistency regularisation methods are simple and can easily be scaled up to large data sets. Of the consistency regularisation methods, Mean-Teacher [32] is the most representative example, containing two identical models which are fed with inputs augmented with different Gaussian noises. The first model learns to match the target output of the second model, while the second model uses an exponentially moving average of parameters of the first model. The state-of-the-art SSL methods [2] [31] combines two categories: entropy minimisation and consistency regularisation.

SSL in segmentation In semi-supervised image segmentation, consistency regularisation is commonly used [35] [21] [8] [14] [10] [11] where different data augmentation techniques

are applied at the input level. Another related work [22] forces the model to learn rotation invariant predictions. Apart from augmentation at the input level, recently, feature level augmentation has gained popularity for consistency based SSL segmentation [28, 16]. Apart from consistency regularisation methods in medical imaging, there also have been other attempts, including the use of generative models for creating pseudo data points for training [3] [5] and different auxiliary tasks as regularisation [17] [6]. Since our method is a new consistency regularisation method, we focus on comparing with state-of-the-art consistency regularisation methods.

III. METHODS

A. Background

Prediction Confidence and Effective Receptive Field We introduce how to control the prediction confidence by controlling the effective receptive field (ERF). ERF [23] measures the size of the effective area at the centre of receptive field and it impacts the most on the prediction confidence of the central pixel of the receptive field. As found in [23], larger ERF means the model can effectively take a larger area of the image into account during inference of decision making, resulting in higher prediction confidence at the centre, meanwhile, smaller ERF leads to less confident prediction on the central pixel due to the lack of visual information of neighbouring pixels. We also show the relationship between ERF and prediction confidence with an example in Fig3. More importantly, ERF is highly affected by the network architecture. In particular, the dilated convolutional layer can increase the ERF to an extent dependent on the dilation rate [23]. Skip-connections conversely can shrink the ERF, though the extent of this effect is as yet unknown [23]. We are therefore inspired by [23] to design a network to control the ERF, in order to deliberately change the prediction confidence.

Overview of MisMatch In this paper, we learn to change prediction confidence by controlling the ERF for consistency regularisation. In order to create a paired predictions with different confidences for consistency regularisation, our strategy is to raise the confidence of one prediction and reduce the confidence of the other prediction, we also compare our strategy with other possible strategies in an ablation study in later section VI. As introduced in the last section, the prediction confidence can be affected by the ERF while the ERF is decided by the network topology. More specifically, we use the dilated convolutional layer to raise the ERF on one hand, and we use skip-connections to decrease the ERF on the other hand. However, we do not know how much confidence should be changed at each pixel. To address this, we introduce soft attention mechanism to learn the magnitude of the confidence change for each pixel. Now we introduce how we achieve this in the next section.

B. Architecture of Mismatch

As shown in Fig.4, MisMatch is a framework which can be integrated into any encoder-decoder based segmentation architecture. In this paper, we use U-net [30] due to its popularity in medical imaging. Our U-net based MisMatch

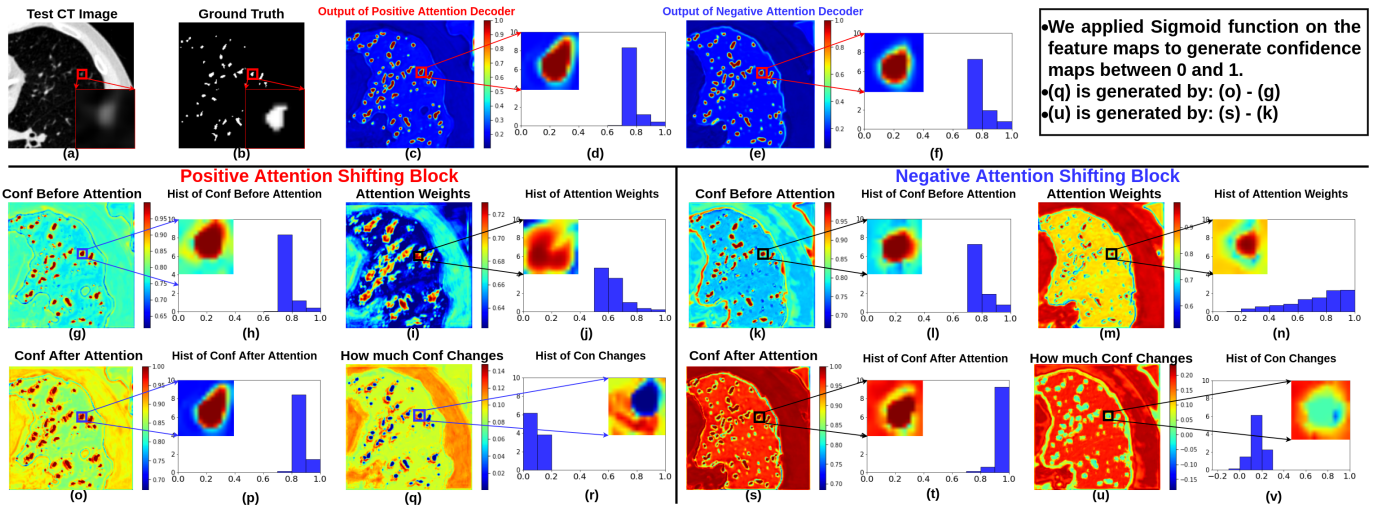


Fig. 2. Visualisation of confidences in the last positive attention shifting decoder and the last negative attention shifting decoder. We focus on the zoomed-in regions on the foreground area containing one vessel. As shown in (p) from the positive attention shifting block, the confidence on the foreground has been raised that even the surrounding areas outside the foreground contour have a high confidence as the foreground. Meanwhile, the confidence on the centre of the foreground remains high as the confidence is already high at the central areas before positive attention is applied. As for the negative attention shifting block, as shown in (t), the confidence on the peripheral areas on the foreground has been decreased as shown in green and blue colours. Additionally, the difference values are negative (see the colour bars in (v)). As shown in the attention weights in (j) and (n), both the attention blocks focus on changing the confidence on the edges of the foreground, this is because the edges are normally the most ambiguous areas.

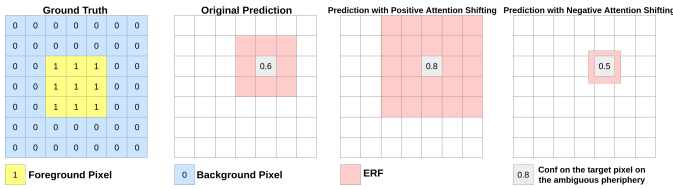


Fig. 3. An example showing how the size of ERF affects the prediction confidence in binary segmentation, especially for pixels close to the peripheral ambiguous areas.

(**Fig 4**) has two components, an encoder (f_e) and a two-head decoder (f_{d1} and f_{d2}). The first decoder (f_{d1}) comprises of a series of *Positive Attention Shifting Blocks*, which shifts more attention towards the foreground RoI area, resulting in higher-confidence predictions on the RoI. The second decoder (f_{d2}) containing a series of *Negative Attention Shifting Blocks*, shifts less attention towards the RoI, resulting in lower-confidence predictions on the RoI. In essence MisMatch has some similarities with morphological operations (e.g. erosion, dilation). However in contrast to morphological operations which simply remove/add boundary pixels using local neighbouring information, MisMatch considers global information and realistically skews the prediction confidence distribution between foreground and background classes using attention mechanisms.

C. Positive Attention Shifting Block

Positive Attention Shifting Block aims at increasing the prediction confidence on the foreground which is our regions of the interest, therefore the name "positive". In a standard U-net, a block ($f(\cdot)$) in the decoder comprises two consecutive convolutional layers with kernel size (K) 3 followed by ReLU

and normalisation layers. If the input of $f(\cdot)$ is x and the output of $f(\cdot)$ is $f(x)$, to increase the high confidence area of $f(x)$, we would aim to generate an attention mask with a larger ERF than the ERF of $f(x)$. To do so, we add a parallel side branch $f'(\cdot)$ next to the main branch $f(\cdot)$. The side branch intakes x but outputs $f'(x)$ with a larger ERF. We apply Sigmoid on the output of the side branch as an attention mask to increase the confidence of $f(x)$. The new block containing both $f(\cdot)$ and $f'(\cdot)$ is our proposed Positive Attention Shifting Block (PASB). The side branch of the PASB is a dilated convolutional layer with dilation rate 5.

1) *ERF size in Positive Attention Shifting Block*: Given the size of ERF of n^{th} layer as, \sqrt{n} [23], which is the input x , as output from the previous layer. The ERF of $f(x)$ is $ERF_{f(x)} = K\sqrt{n+2}$. To make sure the ERF of $f'(x)$ is larger than $K\sqrt{n+2}$:

$$\frac{ERF_{f'(x)}}{ERF_{f(x)}} = \frac{K'}{K} \sqrt{\frac{1}{1 + \frac{1}{n+1}}} > \lim_{n \rightarrow +0} \frac{K'}{K} \sqrt{0.5} > 1 \quad (1)$$

From Eq1, we find $K' > \frac{1}{\sqrt{0.5}}K \approx 1.5K$. We double the condition as our design choice, then K' is 9 when $K = 3$. However, the large kernel sizes significantly increase model complexity. To avoid this, we use a dilated convolutional layer to achieve K' at 9, which requires a dilation rate 5. As the side branch has a larger ERF than the main branch, it can raise the confidence on the foreground of the main branch. Previous work [36, 34] has reported similar uses of a dilated convolutional layer to increase the ERF for other applications, without explaining the rationale for their use.

D. Negative Attention Shifting Block

Negative Attention Shifting Block aims at decreasing the prediction confidence on the foreground which is our regions

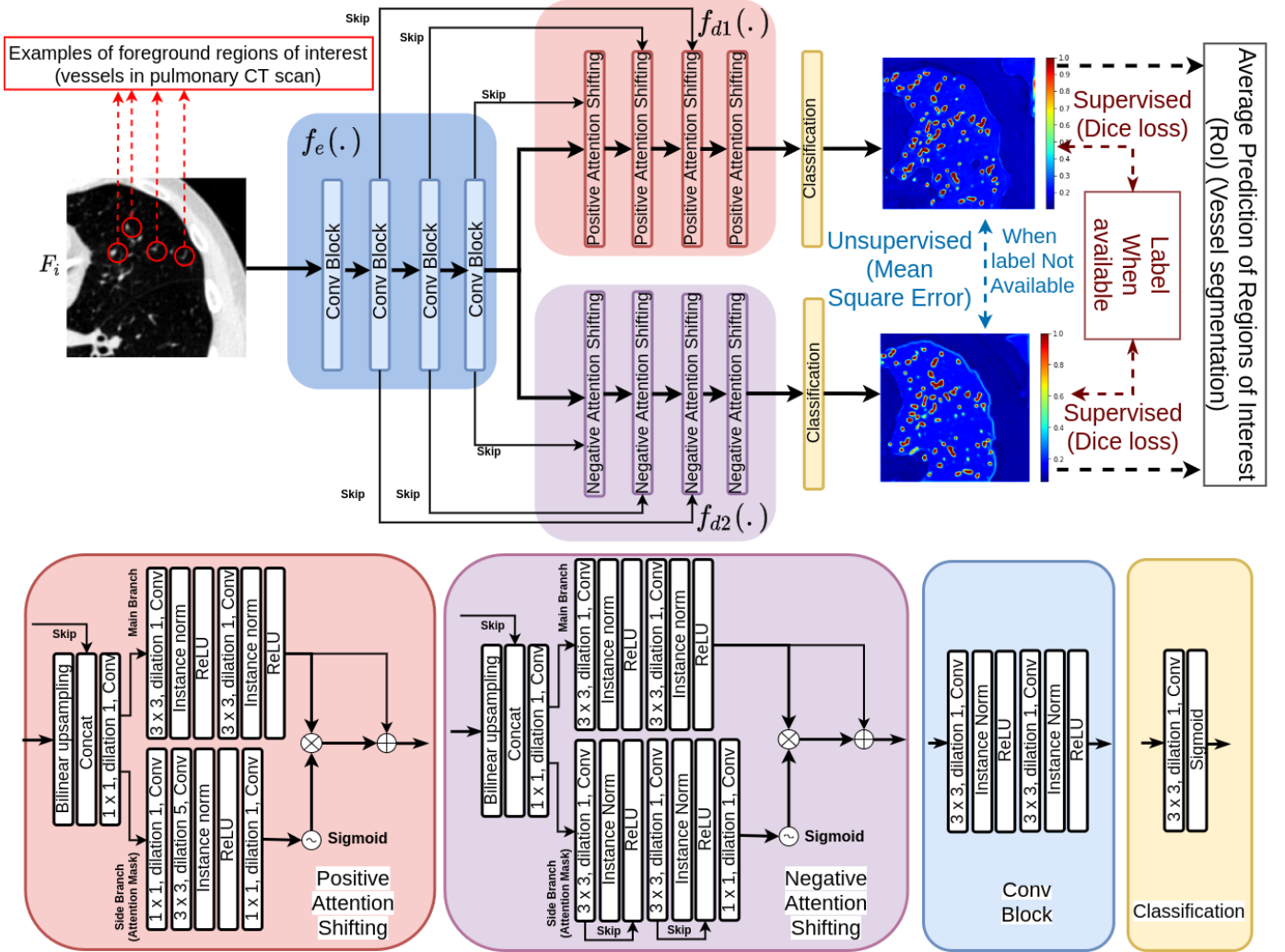


Fig. 4. MisMatch (U-net based) learns confidence invariant predictions on RoI: decoder f_{d1} leads to higher-confidence detection of RoI and decoder f_{d2} leads to lower-confidence detection of RoI. The final prediction is the average between outputs of f_{d1} and f_{d2} . Any other encoder-decoder segmentation network could be used.

of the interest, therefore the name "negative". Following PASB, we design the Negative Attention Shifting Block (NASB) again as two parallel branches. In NASB, we aim to shrink the high confidence area of the $f(x)$ in order to produce a lower confidence prediction of the main branch. In the side branch in NASB, we use the same architecture as the main branch, but with skip-connections as skip-connections restrict the growth of the ERF with increasing depth [23].

1) *ERF size in Negative Attention Shifting Block*: Neural networks with residual connections are equivalent to an ensemble of networks with short paths where each path follows a binomial distribution [33]. If we define p as the probability of the model going through a convolutional layer and $1 - p$ as the probability of the model skipping the layer, then each short path has a portion of $\binom{N}{k} p^k (1 - p)^{N-k}$, contributing to the final ERF. If we assume p is 0.5, the ERF of the side branch is guaranteed to be smaller than the ERF of the main

branch, see Eq.2.

$$\begin{aligned} \frac{ERF_{f'(x)}}{ERF_{f(x)}} &= 0.25 \sqrt{\frac{1}{1 + \frac{2}{n}}} + 0.5 \sqrt{\frac{1}{1 + \frac{1}{n+1}}} + 0.25 \\ &< \lim_{n \rightarrow +\infty} 0.25 + 0.5 + 0.25 = 1 \end{aligned} \quad (2)$$

As the side branch has a smaller ERF than the main branch, it can reduce the confidence on the foreground of the main branch.

E. Loss Functions

We use a streaming training setting to avoid over-fitting on limited labelled data so the model doesn't repeatedly see the labelled data during each epoch. When a label is available, we apply a standard Dice loss [25] between the output of each decoder and the label. When a label is not available, we apply a mean squared error loss between the outputs of the two decoders. This consistency regularisation is weighted by hyper-parameter α .

IV. A PROBABILISTIC INTERPRETATION OF CONSISTENCY BASED SSL AND MISMATCH

In a typical consistency based SSL [31], the convolutional neural network (CNN) model (θ) first predicts the unlabelled data x_u as y_u . One can see y_u as a prediction with “standard” confidence. Then a strong perturbation (e.g. CutMix([37])) is applied on x_u to make it \tilde{x}_u , the model makes the other prediction of \tilde{x}_u as \tilde{y}_u . \tilde{y}_u can be seen as a prediction with “much lower” confidence because \tilde{x}_u is much more difficult to classify than x_u . Then a consistency regularisation (e.g. mean-squared error) is applied between \tilde{y}_u and y_u . Ignoring the data label for notational simplicity, then the maximum a posteriori (MAP) estimation for the likelihood of output $p(y_u|x_u)$ is:

$$p(y_u|x_u) = \int p(y_u|\theta)p(\theta|x_u)d\theta \quad (3)$$

We denote the prediction with perturbed unlabelled data as \tilde{y}_u , perturbed image as \tilde{x}_u , data augmentation as σ , then the MAP estimate of the likelihood of $p(\tilde{y}_u|x_u)$ becomes:

$$p(\tilde{y}_u|x_u) = \int p(\tilde{y}_u|\theta)p(\theta|\tilde{x}_u)p(\tilde{x}_u|x_u)p(\tilde{x}_u|\sigma)d\theta \quad (4)$$

where the data augmentation method σ (e.g. rotation, CutMix) is pre-determined, and typically operates at the image-level without considering spatial correlations among pixels. Such perturbations are not adaptive across pixels and not adaptive for different images, whereas spatial correlations contain rich information for segmentation. Thus, as shown in Eq 4, the perturbation σ is denoted as independent from the image x_u .

Our aim was to create paired predictions with different confidences for consistency regularisation. The action of changing a prediction confidence is a crucial step to achieve a consistency driven SSL in segmentation. To generate an action that leads to a change of prediction confidence: 1) the action should be executed at the feature level [28]; 2) the action should be adaptive across pixels, considering spatial correlations of pixels; 3) the action should not change the pixel-wise label [16] so that the predictions have paired spatial correspondence with each other at the pixel-level. A commonly used method of modelling such an action is a multivariate distribution, however its representation power is limited. We use an overparameterised CNN to directly learn how much confidence should be changed at each pixel, conditioning on the whole image. To achieve this, we add extra parameters $\tilde{\theta}$ and translate Eq. 3 into:

$$p(\tilde{y}_u|x_u) = \int p(\tilde{y}_u|\theta, \tilde{\theta})p(\tilde{\theta}|x_u)p(\theta|x_u)d\tilde{\theta}d\theta \quad (5)$$

Following [36], we design $\tilde{\theta}$ as an attention module and $p(\tilde{\theta}|x_u)$ as the learnt attention mask which will be element-wise multiplied with $p(\theta|x_u)$ to change each pixel’s confidence. Unlike previous SSL approaches which decrease prediction confidence by injecting perturbations, we both increase and decrease prediction confidences.

V. EXPERIMENTS

We perform three sets of experiments: 1) comparisons with baselines including supervised learning and state-of-the-art

SSLs [31, 32, 6, 28] using either data or feature augmentation; 2) investigation of the impact of the amount of labelled data and unlabelled data on MisMatch performance; 3) ablation study of the decoder architectures; 4) ablation study on the hyper-parameter, on the CARVE dataset using 5 labelled slices.

A. Implementation

We use Adam optimiser [18]. Hyper-parameters are: $\alpha = 0.002$, batch size 1 (GPU memory: 2G), learning rate $2e-5$, 50 epochs. Each complete training on CARVE takes about 3.8 hours. The final output is the average of the outputs of the two decoders. In testing, we take an average of models saved over the last 10 epochs across experiments. Our code is implemented using Pytorch 1.0 [29].

B. Baselines

In the current study the backbone is a 2D U-net [30] with 24 channels in the first encoder. To ensure a fair comparison we use the same U-net as the backbone across all baselines. The first baseline utilises supervised training on the backbone, is trained with labelled data, augmented with flipping and Gaussian noise and is denoted as “Sup1”. To investigate how unlabelled data improves performance, our second baseline “Sup2” utilises supervised training on MisMatch, with the same augmentation. Because MisMatch uses consistency regularisation, we focus on comparisons with five consistency regularisation SSLs: 1) “mean-teacher” (MT) [32], with Gaussian noise, which has inspired most of the current state-of-the-art SSL methods; 2) the current state-of-the-art model called “FixMatch” (FM) [31]. To adapt FixMatch for a segmentation task, we use Gaussian noise as weak augmentation and “RandomAug” [7] without shearing for strong augmentation. We do not use shearing for augmentation because it impairs spatial correspondences of pixels of paired dense outputs; 3) a state-of-the-art model with multi-head decoder [28] for segmentation (CCT), with random feature augmentation in each decoder [28]. This baseline is also similar to models recently developed [11, 16]; 4) a further recent model in medical imaging [6] using image reconstruction as an extra regularisation (MTA), augmented with Gaussian noise; 5) a U-net with two standard decoders, where we respectively apply erosion and dilation on the features in each decoder, augmented with Gaussian noise (Morph). Our MisMatch model has been trained without any augmentation.

C. Data sets & Pre-processing

CARVE 2014 The Classification of pulmonary arteries and veins (CARVE) dataset [4] has 10 fully annotated non-contrast low-dose thoracic CT scans. Each case has between 399 and 498 images, acquired at various spatial resolutions between (282 x 426) to (302 x 474). 10-fold cross-validation on the 10 labelled cases is performed. In each fold, we split cases as: 1 for labelled training data, 3 for unlabelled training data, 1 for validation and 5 for testing. We only use slices containing more than 100 foreground pixels. We prepare datasets with

TABLE I
MISMATCH (MM) VS BASELINES ON CARVE. METRIC IS INTERSECTION OVER UNION (IOU).

Labelled Slices	Supervised		Semi-Supervised					
	Sup1 [30](2015)	Sup2 Ours(2021)	MTA [6](2019)	MT [32](2017)	FM [31](2020)	CCT [28](2020)	Morph 2021	MM Ours(2021)
5	48.32±4.97	50.75±2.0	54.91±1.82	56.56±2.38	49.30±1.81	52.54±1.74	52.93±2.19	60.25±3.77
10	53.38±2.83	55.55±4.42	57.78±3.66	57.99±2.57	51.53±3.72	55.25±2.52	57.08±2.96	60.04±3.64
30	52.09±1.41	53.98±4.42	60.78±4.63	60.46±3.74	55.16±5.93	60.81±4.09	60.19±4.97	63.59±4.46
50	60.69±2.51	64.79±3.46	68.11±3.39	67.21±3.05	62.91±6.99	65.06±3.42	64.88±3.25	69.39±3.74
100	68.74±1.84	73.1±1.51	72.48±1.61	71.48±1.57	72.58±1.84	72.07±1.75	72.11±1.88	74.83±1.52
Param. (M)	1.8	2.7	2.1	1.88	1.88	1.88	2.54	2.7
Infer.Time(s)	4.1e-3	1.8e-1	7.2e-3	4.3e-3	4.5e-3	1.5e-1	8e-3	1.8e-1

TABLE II
MISMATCH (MM) VS BASELINES ON BRATS. METRIC IS INTERSECTION OVER UNION (IOU).

Unlabelled Slices	Supervised		Semi-Supervised					
	Sup1 [30](2015)	Sup2 Ours(2021)	MTA [6](2019)	MT [32](2017)	FM [31](2020)	CCT [28](2020)	Morph 2021	MM Ours(2021)
3100	53.74±10.19	55.76±11.03	50.53±8.76	55.29±10.21	57.92±12.35	56.61±11.7	53.88±9.99	58.94±11.41
4650	53.74±10.19	55.76±11.03	47.36±6.65	58.32±12.07	54.29±9.69	56.94±10.93	55.82±11.03	60.74±12.96
6200	53.74±10.19	55.76±11.03	50.11±8.00	56.92±12.20	56.78±11.39	57.37±11.74	54.5±9.75	58.81±12.18

differing amounts of labelled slices: 5, 10, 30, 50, 100. We crop 176×176 patches from four corners of each slice. Full label training uses 4 training cases. Normalisation was performed at case wise.

BRATS 2018 BRATS 2018 [24] has 210 high-grade glioma and 76 low-grade glioma MRI cases, each case containing 155 slices. We focus on binary segmentation of whole tumours in high grade cases. We randomly select 1 case for labelled training, 2 cases for validation and 40 cases for testing. We centre crop slices at 176×176 . For labelled training data, we extract the first 20 slices containing tumours with areas of more than 5 pixels. To see the impact of the amount of unlabelled training data, we use 3100, 4650 and 6200 slices respectively. Case-wise normalisation was performed and all modalities were concatenated. We train each model 3 times and take the average.

VI. RESULTS AND DISCUSSION

A. Segmentation Performance

MisMatch consistently and substantially outperforms supervised baselines, the improvement is especially obvious in low data regime. For example, on 5 labelled slices with CARVE, MisMatch achieves 24% improvement over Sup1. MisMatch consistently outperforms previous SSL methods [31, 32, 6, 28] in Table I, across different data sets. Particularly, there exists statistical difference between Mismatch and other baselines when 6.25% labels (100 slices comparing to 1600 slices of full label) are used on CARVE (Table III). Qualitatively, we observed in Fig 7 that, the main performance boost of MisMatch comes from the reduction of false positive detection and the increase of true positive detection.

Interestingly, we found that Sup2 (supervised training on MisMatch without unlabelled data) is a very competitive baseline comparing to previous semi-supervised methods. This might imply that MisMatch can potentially help with the supervised learning as well.

We also found data diversity of training data highly affects the testing performance (Fig 5) in cross-validation experiments. For example, in fold 3, 7 and 8 on CARVE, MisMatch outperforms or performs on-par with the full label training, whereas in the rest folds, MisMatch performs marginally inferior to the full label training. Additionally, more labelled training data consistently produces a higher mean IoU and lower standard deviation (Table II). Lastly, we noticed more unlabelled training data can help with generalisation, until it dominates training and impedes performance (Table II).

TABLE III

P-VALUE BETWEEN MM AND BASELINES. NON-PARAMETRIC MANN-WHITNEY U-TEST. 100 LABELLED SLICES OF CARVE.

Sup1	Sup2	MTA	MT	FM	CCT	Morph
9.13e-5	1.55e-2	4.5e-3	4.3e-4	1.05e-2	1.8e-3	2.2e-3

B. Ablation Studies

We performed ablation studies on the architecture of the decoders of MisMatch with cross-validation on 5 labelled slices of CARVE: 1) “MM-a”, a two-headed U-net with standard convolutional blocks in decoders, the prediction confidences of these two decoders can be seen as both normal confidence, however, they are essentially slightly different because of random initialisation, we denote the decoder of U-net as f_{d0} ; 2) “MM-b”, a standard decoder of U-net and a negative attention shifting decoder f_{d2} , this one can be seen as between normal confidence and less confidence; 3) “MM-c”, a standard decoder of U-net and a positive attention shifting decoder f_{d1} , this one can be seen as between normal confidence and higher confidence; 4) “MM”, f_{d1} and f_{d2} (Ours). As shown in Fig 6, our MisMatch (“MM”) outperforms other combinations in 8 out of 10 experiments and it performs on par with the others in the rest 2 experiments. Among the results when MisMatch outperforms, MisMatch outperforms MM-a by 2%-

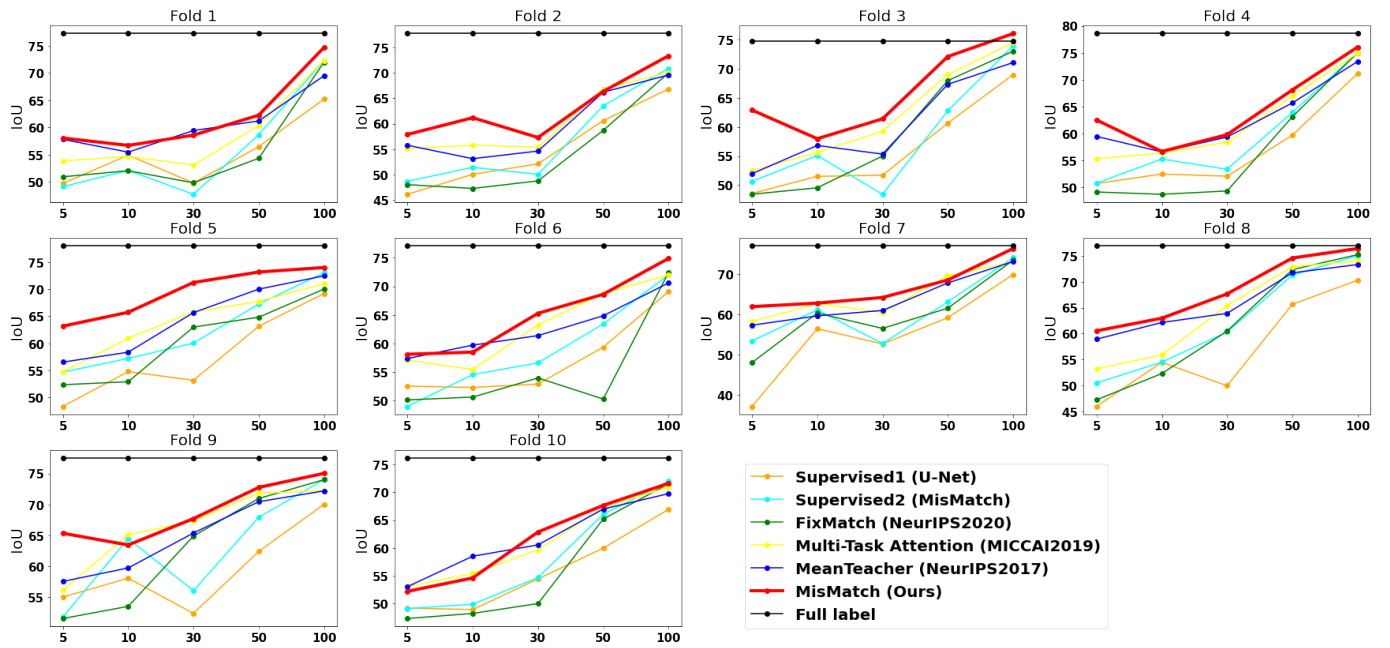


Fig. 5. Full results of 10 fold cross-validation on CARVE. X-axis: number of labelled slices. Y-axis: IoU

14%; outperforms MM-b by 3%-18%; outperforms MM-c by 4%-22%.

We also tested α at 0, 0.0005, 0.001, 0.002, 0.004 with the same experimental setting. The optimal α appears at 0.002 in Table IV.

TABLE IV

ABLATION STUDIES ON ALPHA VALUE USING CARVE WITH 5 LABELLED SLICES.

alpha	0.0	0.0005	0.001	0.002	0.004
IoU	50.75	59.16	59.45	60.25	58.89

C. Effectiveness of Learnt Attention Masks

We visualise the confidences of feature maps before and after attention, attention weights and how much the confidences are changed in Fig2 on CARVE. We focus on zoomed-in area of one vessel. As shown in (c) and (e), the confidence outputs between the two decoders are different, the one from the positive attention decoder has more detected high confidence areas on the top of the anatomy of the interest. As illustrated in (j) and (n), the attention weights in the two decoders are drastically different from each other. More specifically, the attention weights in the negative attention decoder have relatively low values around the edges, as shown in green and blue colours, on the contrary, the attention weights in the positive attention decoder have high values in most of the regions of the interest.

Another evidence supporting the effectiveness of attention blocks are the changes of the confidences as shown in (r) and (v). After positive attention weights are applied on (g), it is clear to see in (r) that the surrounding areas of the originally

detected contours are now also detected as regions of the interest. Besides, in (v), we observe expected negative changes of the confidences around edges caused by the negative attention shifting.

The histograms also support the effectiveness of our learnt attention masks. Between the histograms in (j) and (m), for the high confidence interval between 0.9 and 1.0, the negative attention block has more high confidence pixels than the positive attention block. This is because the negative attention block decreases confidence on foreground, thereby ending up with increasing confidence on background, where background class is the majority class naturally containing more pixels than the foreground class.

D. Confidence and Calibration of Mismatch

Expected Calibration Error To qualitatively study the confidence of MisMatch, we adapt two mostly used metrics in the community, which are Reliability Diagrams and Expected Calibration Error (ECE) [13]. Following [9], we first prepare M interval bins of predictions. In our binary setting to classify the foreground, we use 5 intervals between 0.5 to 1. Say B_m is the subset of all pixels whose prediction confidence is in interval I_m . We define accuracy as how many pixels are correctly classified in each interval. The accuracy of B_m is formally:

$$acc(B_m) = \frac{1}{|B_m|} \sum_{i \in B_m} 1(\hat{y}_i = y_i) \quad (6)$$

Where \hat{y}_i is the predicted label and y_i is the ground truth label at pixel i in B_m . The average confidence within B_m is defined with the use of \hat{p}_i which is the raw probability output of the

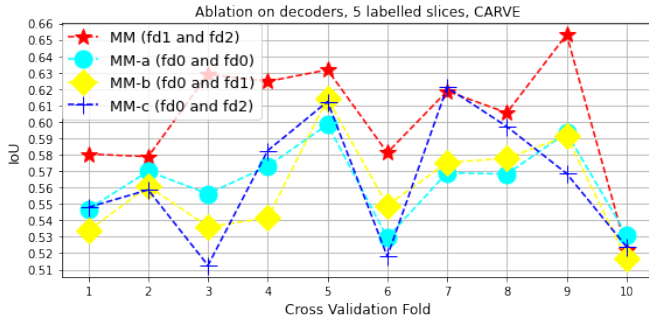


Fig. 6. Ablation studies on decoder architectures, cross-validation on 5 labelled slices with CARVE. MM is ours.

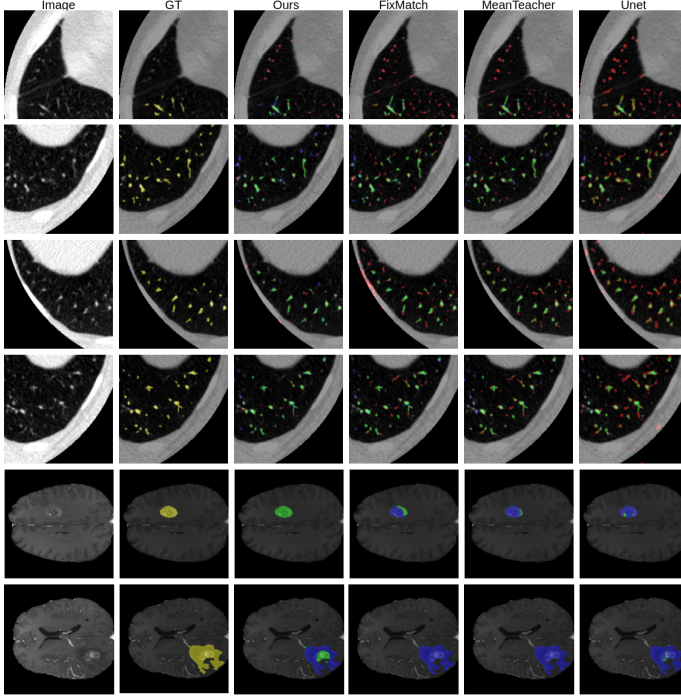
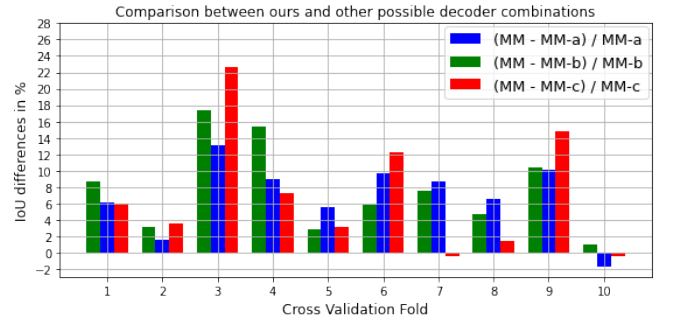


Fig. 7. Visual results. Yellow: ground truth. Red: False Positive. Green: True Positives. Blue: False Negatives. Row 1-4: CARVE. Row 5-6: BRATS

network at each pixel:

$$\text{conf}(B_m) = \frac{1}{|B_m|} \sum_{i \in B_m} \hat{p}_i \quad (7)$$

Ideally, we would like to see $\text{conf}(B_m) = \text{acc}(B_m)$, which means the network is perfectly calibrated and the predictions are completely trustworthy. To assess how convincing the prediction confidences are, we calculate the gap between confidence and accuracy as Expected Calibration Error (ECE):

$$\text{ECE} = \sum_{m=1}^M \frac{|B_m|}{n} |\text{acc}(B_m) - \text{conf}(B_m)| \quad (8)$$

MisMatch is well-calibrated and effectively learns to change prediction confidence As shown in Fig8, both positive attention shifting decoder and negative attention shifting decoder are better calibrated than the plain U-net. Especially, positive attention shifting decoder produces over-confident

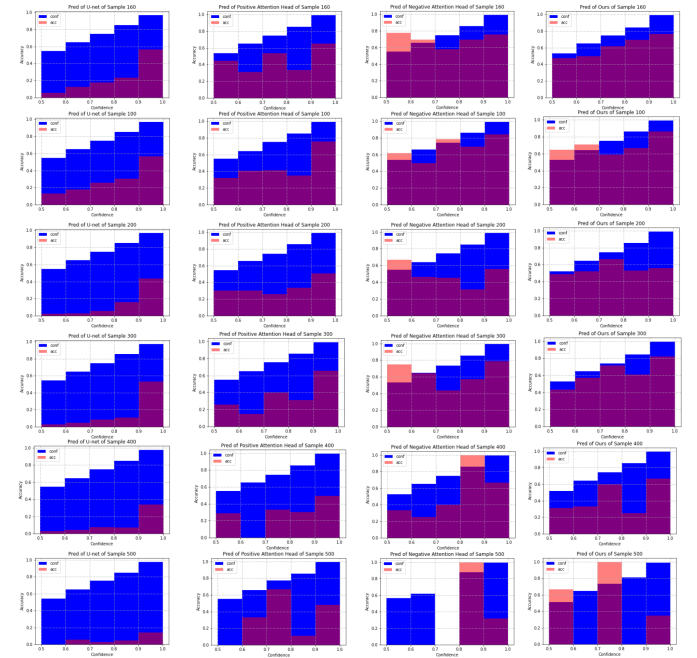


Fig. 8. Reliability diagrams [13] from experiments on 50 labelled slices with CARVE. Blue: Confidence. Red: Accuracy. Each row is on one testing image. X-axis: bins of prediction confidences. Y-axis: accuracy. Column 1: U-net. Column 2: outputs of positive attention decoders. Column 3: outputs of negative attention decoders. Column 4: average outputs of the two decoders. The smaller the gap between the accuracy and the confidence, the better the network is calibrated.

predictions. Meanwhile, negative attention shifting decoder produces under-confident predictions for a few confidence intervals. This verifies again that MisMatch can effectively learn to differently change the prediction confidences of the same testing images.

Robustness of MisMatch Against Calibration Errors As shown in the scatter plot (Fig9) of paired IoU and corresponding Expected Calibration Error (ECE) of all of the testing images in cross-validation experiments on 50 labelled slices of CARVE, higher calibration errors correlate positively with low segmentation accuracy. In general, MisMatch has predictions with less calibration errors and higher IoU values. As shown in the 2nd order regression curves for each trend, MisMatch appears to be more robust against calibration error, as the fitted curve of U-net has a much more steep slope than MisMatch. In other words, with the increase of calibration error, MisMatch

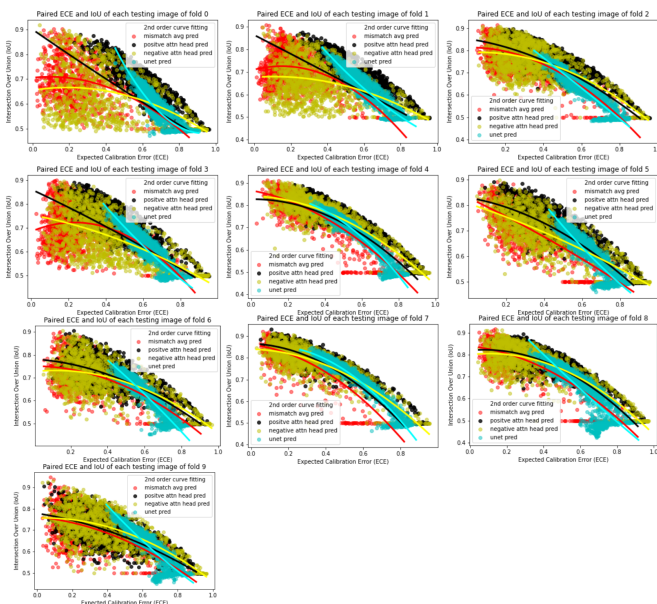


Fig. 9. Expected calibration error [13] against accuracy in 10-fold cross-validation experiments on 50 labelled slices with CARVE. Y-axis: IoU. X-axis: ECE. Each calibration error is calculated from the gap between the confidence and accuracy for each testing image. Each data point in this figure is one testing image. The fitted 2nd order trends of our MisMatch are flatter than U-net, meaning MisMatch is more robust against the calibration error.

suffers less performance drops.

VII. CONCLUSION

We propose MisMatch, an augmentation-free SSL, to overcome the limitations associated with consistency-driven SSL in medical image segmentation. In lung vessel segmentation tasks, the acquisition of labels can be prohibitively time-consuming. For example each case may take 1.5 hours of manual refinement with semi-automatic segmentation[4]. Longer timeframes may be required for cases with severe disease. MisMatch however shows strong clinical utility by reducing the number of training labels required by more than 90%. MisMatch requires 100 slices of one case for training whereas the fully labelled dataset comprises 1600 slices across 4 cases. MisMatch when trained on just 10% of labels achieves a similar performance (IoU: 75%) to models that are trained with all available labels (IoU: 77%). Although MisMatch achieves superior performance over previous methods, it suffers from increased model complexity. Future work will extend MisMatch to multi-class 3D tasks incorporating uncertainty quantification as well as improving model efficiency. We also aim to enhance MisMatch by combining it with existing temporal ensemble techniques [32].

REFERENCES

[1] Ben Athiwaratkun et al. “There Are Many Consistent Explanations of Unlabeled Data: Why You Should Average”. In: *International Conference on Learning Representations (ICLR)* (2019).

[2] David Berthelot et al. “REMIXMATCH: SEMI-SUPERVISED LEARNING WITH DISTRIBUTION ALIGNMENT AND AUGMENTATION ANCHORING”. In: *International Conference On Learning Representation (ICLR)* (2020).

[3] Krishna Chaitanya et al. “Semi-supervised and Task-Driven Data Augmentation”. In: *Information Processing In Medical Imaging (IPMI)* (2019).

[4] Jean-Paul Charbonnier et al. “Automatic Pulmonary Artery-Vein Separation and Classification in Computed Tomography Using Tree Partitioning and Peripheral Vessel Matching”. In: *IEEE Transaction on Medical Imaging* (2015).

[5] Chen Chen et al. “Realistic Adversarial Data Augmentation for MR Image Segmentation”. In: *International Conference on Medical Image Computing and Computer-Assisted Intervention (MICCAI)* (2020).

[6] Shuai Chen et al. “Multi-task Attention-Based Semi-supervised Learning for Medical Image Segmentation”. In: *International Conference on Medical Image Computing and Computer-Assisted Intervention (MICCAI)* (2019).

[7] Ekin D. Cubuk et al. “RandAugment: Practical automated data augmentation with a reduced search space”. In: *Neural Information Processing Systems (NeurIPS)* (2020).

[8] Wenhui Cui et al. “Semi-Supervised Brain Lesion Segmentation with an Adapted Mean Teacher Model”. In: *Information Processing in Medical Imaging (IPMI)* (2019).

[9] Morris DeGroot and Stephen Feinberg. “The comparison and evaluation of forecasters”. In: *The statistician* (1983).

[10] Kang Fang and Wu-Jun Li. “DMNet: Difference Minimization Network for Semi-supervised Segmentation in Medical Images”. In: *International Conference on Medical Image Computing and Computer-Assisted Intervention (MICCAI)* (2020).

[11] Geoff French et al. “Semi-supervised semantic segmentation needs strong, varied perturbations”. In: *British Machine Vision Conference (BMVC)* (2020).

[12] Yves Grandvalet and Yoshua Bengio. “Semi-supervised Learning by Entropy Minimization”. In: *Neural Information Processing Systems (NeurIPS)* (2004).

[13] Chuan Guo et al. “On Calibration of Modern Neural Networks”. In: *International Conference on Machine Learning (ICML)* (2017).

[14] Wenlong Hang et al. “Local and Global Structure-Aware Entropy Regularized Mean Teacher Model for 3D Left Atrium Segmentation”. In: *International conference on medical image computing and computer assisted intervention (MICCAI)* (2020).

[15] Ahmet Iscen et al. “Label Propagation for Deep Semi-supervised Learning”. In: *Computer Vision and Pattern Recognition (CVPR)* (2019).

[16] Zhanghan Ke et al. “Guided Collaborative Training for Pixel-wise Semi-Supervised Learning”. In: *European Conference on Computer Vision (ECCV)* (2020).

- [17] Hoel Kervadec et al. "Curriculum Semi-supervised Segmentation". In: *International Conference on Medical Image Computing and Computer-Assisted Intervention (MICCAI)* (2019).
- [18] Diederik P. Kingma and Jimmy Ba. "Adam: A Method for Stochastic Optimization". In: *International Conference on Learning Representation (ICLR)* (2015).
- [19] Diederik P. Kingma et al. "Semi-supervised Learning with Deep Generative Models". In: *Advanced in Neural Information Processing System (NeurIPS)* (2014).
- [20] Dong-Hyun Lee. "Pseudo-Label : The Simple and Efficient Semi-Supervised Learning Method for Deep Neural Networks". In: *ICML workshop on Challenges in Representation Learning* (2013).
- [21] Kang Li et al. "Dual-Teacher: Integrating Intra-domain and Inter-domain Teachers for Annotation-Efficient Cardiac Segmentation". In: *International Conference on Medical Image Computing and Computer-Assisted Intervention (MICCAI)* (2020).
- [22] Xiaomeng Li et al. "Semi-supervised Skin Lesion Segmentation via Transformation Consistent Self-ensembling Model". In: *British Machine Vision Conference (BMVC)* (2018).
- [23] Wenjie Luo et al. "Understanding the Effective Receptive Field in Deep Convolutional Neural Networks". In: *Neural Information Processing Systems (NeurIPS)* (2016).
- [24] Bjoern H. Menze et al. "The Multimodal Brain Tumor Image Segmentation Benchmark (BRATS)". In: *IEEE Transaction on Medical Imaging* (2015).
- [25] Fausto Milletari, Nassir Navab, and Seyed-Ahmad Ahmadi. "V-Net: Fully Convolutional Neural Networks for Volumetric Medical Image Segmentation". In: *International Conference on 3D Vision (3DV)* (2016).
- [26] Takeru Miyato et al. "Virtual Adversarial Training: A Regularization Method for Supervised and Semi-Supervised Learning". In: *IEEE Transactions on Pattern Analysis and Machine Intelligence* (2017).
- [27] Avital Oliver et al. "Realistic Evaluation of Deep Semi-Supervised Learning Algorithms". In: *Neural Information Processing Systems (NeurIPS)* (2018).
- [28] Yassine Ouali, Céline Hudelot, and Myriam Tami. "Semi-Supervised Semantic Segmentation with Cross-Consistency Training". In: *Computer Vision and Pattern Recognition (CVPR)* (2020).
- [29] Adam Paszke et al. "PyTorch: An Imperative Style, High-Performance Deep Learning Library". In: *Neural Information Processing System (NeurIPS)* (2019).
- [30] Olaf Ronneberger, Philipp Fischer, and Thomas Brox. "U-Net: Convolutional Networks for Biomedical Image Segmentations". In: *International conference on medical image computing and computer assisted intervention (MICCAI)* (2015).
- [31] Kihyuk Sohn et al. "FixMatch: Simplifying Semi-Supervised Learning with Consistency and Confidence". In: *Neural Information Processing Systems (NeurIPS)* (2020).
- [32] Antti Tarvainen and Harri Valpola. "Mean teachers are better role models: Weight-averaged consistency targets improve semi-supervised deep learning results". In: *Neural Information Processing Systems (NeurIPS)* (2017).
- [33] Andreas Veit, Michael Wilber, and Serge Belongie. "Residual Networks Behave Like Ensembles of Relatively Shallow Networks". In: *Neural Information Processing Systems (NeurIPS)* (2016).
- [34] Yunchao Wei et al. "Revisiting Dilated Convolution: A Simple Approach for Weakly- and SemiSupervised Semantic Segmentation". In: *Computer Vision and Pattern Recognition (CVPR)* (2018).
- [35] Junshen Xu et al. "Semi-supervised Learning for Fetal Brain MRI Quality Assessment with ROI Consistency". In: *International Conference on Medical Image Computing and Computer-Assisted Intervention (MICCAI)* (2020).
- [36] Mou-Cheng Xu et al. "Learning To Pay Attention To Mistakes". In: *British Machine Vision Conference (BMVC)* (2020).
- [37] Sangdoon Yun et al. "CutMix: Regularization Strategy to Train Strong Classifiers with Localizable Features". In: *International Conference on Computer Vision (ICCV)* (2019).